PCCP

PAPER

View Article Online
View Journal | View Issue

Cite this: *Phys. Chem. Chem. Phys.*, 2016, **18**, 1245

Using the C–O stretch to unravel the nature of hydrogen bonding in low-temperature solid methanol–water condensates

Anita Dawes,* Nigel John Mason and Helen Jane Fraser

Received 4th September 2015,
Accepted 3rd December 2015

DOI: 10.1039/c5cp05299h

www.rsc.org/pccp

Transmission infrared spectroscopy has been used in a systematic laboratory study to investigate hydrogen bonding in binary mixtures of CH_3OH and H_2O, vapour deposited at 30 K, as a function of CH_3OH/H_2O mixing ratio, R. Strong intermolecular interactions are evident between CH_3OH and H_2O with infrared band profiles of the binary ices differing from that of the pure components and changing significantly with R. Consistent evidence from the O–H and C–H band profiles and detailed analysis of the C–O stretch band reveal two different hydrogen bonding structural regimes below and above R = 0.6–0.7. The vapour deposited solid mixtures were found to exhibit behaviour similar to that of liquids with evidence of inhomogeneity and higher coordination number of hydrogen bonds that are concentration dependent. The C–O stretch band is found to consist of three components around 1039 cm^{-1} ('blue'), 1027 cm^{-1} ('middle') and 1011 cm^{-1} ('red'). The 'blue' and 'middle' components corresponding to environments with CH_3OH dominating as a proton donor (PD) and proton acceptor (PA) respectively reveal preferential bonding of CH_3OH as a PA and H_2O as a PD in the mixtures. The 'red' component is only present in the presence of H_2O and has been assigned to the involvement of both lone pairs of electrons on the oxygen atom of CH_3OH as a PA to two PD H_2O atoms. Cooperative effects are evident with concurrent blue-shifts in the C–H stretching modes of CH_3OH below R = 0.6 indicating CH_3 group participation in hydrogen bonding.

1 Introduction

Solid methanol (CH_3OH) is an important constituent of ices in the interstellar medium (ISM). It is the precursor for the formation of many of the complex organic molecules (COMs) observed in the ISM, both in the gas and the solid phases; molecules that subsequently became incorporated into cometary ices during the formation of planetary systems, with some believed to lead to the formation of prebiotic molecules responsible for the chemical origins of life.[1–4] CH_3OH has been observed in comets[5–7] and on the surfaces of trans-Neptunian objects,[8–10] that are believed to be preserved from the primordial cloud and planetary accretion disk that formed our Solar System. In dense molecular clouds, from which stars are formed, CH_3OH is observed to be one of the most abundant constituents of ices after H_2O and CO.[11–14] Theoretical and experimental evidence suggests that interstellar CH_3OH forms exclusively in the condensed phase on the surfaces of dust grains in dense molecular clouds, *via* successive hydrogenation of CO.[15–20] However wide variations in the abundance of solid CH_3OH in the ISM are observed, ranging from 5 to 30% relative to H_2O and there is still much ambiguity in determining CH_3OH abundances and the degree of mixing with H_2O due to the overlapping of observed CH_3OH vibrational absorption bands with H_2O and silicate absorption features.

The interpretation of observational infrared (IR) spectra of ices relies heavily on laboratory infrared absorption spectra of ice analogues grown under controlled experimental conditions. IR spectroscopy of molecular ices provides a powerful tool in the identification of species and interpretation of the structure and morphology of interstellar ices, since the IR spectra are highly sensitive to the ice temperature, composition, and mixing ratio of the molecular components, which are all intrinsically linked to the intermolecular interactions. Though a number of laboratory studies have been reported for the purposes of constraining methanol abundances from observational spectra,[21–26] detailed and systematic laboratory studies of mixtures/layers of solid H_2O and CH_3OH are still limited. Inspired by the need for such data to interpret observational spectra presented by Suutarinen *et al.*[27] we have carried out a detailed, systematic laboratory spectroscopic study of mixtures of vapour deposited CH_3OH and H_2O, at 30 K,

Department of Physical Sciences, The Open University, Walton Hall, Milton Keynes, MK7 6AA, UK. E-mail: Anita.Dawes@open.ac.uk; Fax: +44 (0)1908 6 54192; Tel: +44 (0)1908 6 54241

as a function of CH_3OH/H_2O ratio. Whilst from an astronomical perspective, the shape and the intensity variations in the O–H and C–H stretching frequencies were sufficient to estimate CH_3OH abundances in Suutarinen *et al.*,[27] the CH_3OH/H_2O ratio could not be constrained and chemical knowledge is required to understand the significance of the spectral changes and link spectral bands, including the most indicative C–O stretch. Therefore this paper focuses not so much on the spectra, but what the spectra can inform us, from a chemical perspective, about the hydrogen bonding and intermixing of the two molecules, H_2O and CH_3OH, as a function of CH_3OH dilution in H_2O.

From a Physical Chemistry perspective, there has been considerable interest in CH_3OH as it is the prototype molecule for hydrogen-bonding alcohols.[28] CH_3OH, has attracted a lot of attention in both computational and experimental studies of hydrogen bonding and mixing in liquids, particularly with H_2O. It is well known from laboratory and computational physical chemistry investigations that both CH_3OH and H_2O form strong hydrogen bonds both as pure constituents and in mixtures, interacting strongly with one another. Hydrogen bonding causes shifts in the vibrational frequencies of the functional groups that they are associated with and it is therefore possible to glean much about the structure and morphology of condensed ices from their infrared spectra. In CH_3OH the vibrational spectra of the O–H, C–H and the C–O stretch are sensitive to the interaction between nearest neighbours. The interactions between CH_3OH and H_2O have been studied in mixed CH_3OH/H_2O liquids,[29–32] heterodimers[33–35] and small clusters both in the gas phase and in matrix isolation studies,[33,34] supported with extensive computational studies.[36–44] The O–H stretch has been used extensively to study hydrogen bonding between H_2O and CH_3OH in dimers, matrix isolation and in clusters, however, in the bulk condensed and liquid phases this poses a problem as the broad absorption bands due to the O–H stretching frequencies of both CH_3OH and H_2O overlap. Therefore to better understand the $CH_3OH\cdots H_2O$ interactions in the bulk solid phase, we focus our analysis in this paper on the C–O stretch of CH_3OH.

The C–O stretch is also sensitive to hydrogen bonding, however, few studies have concentrated on this band.[31,32] It is a favourable band for the study of mixtures with H_2O in the solid (and liquid) phase as it does not overlap with any of the H_2O features and is therefore useful in the interpretation of astronomical spectra. However, observationally this band has not yet been exploited as it lies on a strong interstellar silicate absorption band[21,22,45] which until recently has been difficult to subtract. Nevertheless, in this paper we focus our attention primarily on the C–O stretch band of CH_3OH and the effect the mixing ratio between CH_3OH and H_2O has on the band profile. We wish assess whether the C–O stretch band of CH_3OH can be used as an observational tool to infer the degree of mixing in interstellar ices, particularly with higher sensitivity of newly emerging telescopes that would also enable the simultaneous observation of the C–O, C–H and O–H regions of the spectrum with a single telescope, such as the James Webb Space Telescope.[27] Therefore the primary focus of this paper is that, in order to better inform the Astronomy community, we wish to understand the physico-chemical nature of the intermolecular interactions within the bulk mixed CH_3OH and H_2O low-temperature condensed ice films.

2 Experimental

The experiments were carried out using a high vacuum chamber, with a base pressure of 1×10^{-9} mbar. A 1.5 cm diameter infrared transmitting ZnSe substrate, mounted in a copper sample holder was cooled using a closed cycle helium cryostat (Sumitomo) to temperatures of 30 K. CH_3OH (liquid, Sigma-Aldrich $\geq$99.9% HPLC grade) and H_2O (liquid, triply distilled, deionised) samples were pre-mixed in the gas dosing line after three freeze–pump–thaw cycles. The gas line pressures were held below 10 mbar to avoid condensation of H_2O. Ice films were grown by background filling the vacuum chamber and maintaining a pressure of 1×10^{-7} mbar during deposition using a needle valve to set the flow of gases into the chamber. Ices were grown at a rate of approximately 0.1 ML s^{-1} and all samples were around 100 nm thick as determined from the infrared spectra. Under these conditions the pressure drop in the gas line during deposition was negligible. The partial pressures in the gas line were used as a rough indicator of the sample ratios, however due to differences in the vapour pressure between CH_3OH and H_2O and adsorption–exchange processes on the stainless steel walls of the gas line, the final sample ratios did not entirely agree with the ratios of the pre-mixed gases. Therefore the exact ratios of the mixed ices were subsequently determined from the infrared spectra by calculating the column densities from the integrated absorbance of two bands of CH_3OH and two bands of H_2O, as described in Section 2.1. Infrared spectra of the CH_3OH and H_2O ice mixtures were measured using a Thermo Nicolet NEXUS FTIR spectrometer in the range 4000–800 cm^{-1} at 1 cm^{-1} resolution and averaging together 512 scans.

2.1 Determining the CH_3OH/H_2O ratio, *R*

The $CH_3OH:H_2O$ ratios were determined by calculating the CH_3OH and H_2O column densities from the infrared absorption spectra. The column density N_i (molecules cm^{-2}) of a molecular species i is determined using the Beer–Lambert law:

$$I_t(\bar{\nu}) = I_0(\bar{\nu})e^{-\sigma_i(\bar{\nu})N_i} \quad (1)$$

where $I_0(\bar{\nu})$ and $I_t(\bar{\nu})$ are the incident and the transmitted intensities at wavenumber $\bar{\nu}$ (cm^{-1}) and $\sigma_i(\bar{\nu})$ (cm^2) is the absorption cross section for a given molecular species i.

Rearranging eqn (1), we get

$$\ln\left(\frac{I_0(\bar{\nu})}{I_t(\bar{\nu})}\right) = \tau(\bar{\nu}) = \sigma_i(\bar{\nu})N_i \quad (2)$$

where $\tau(\bar{\nu})$ is the optical depth as a function of frequency $\bar{\nu}$ (cm^{-1}) which is obtained from the absorbance (log scale) measured by the FTIR spectrometer and converted to optical depth (ln scale) by multiplying by ln(10).

Integrating eqn (2) over the absorption band for a given vibrational transition and rearranging, gives the column density

$$N_i = \frac{1}{A_i}\int \tau(\bar{\nu})\mathrm{d}\bar{\nu} \quad (3)$$

where the integral $\int\tau(\bar{\nu})\mathrm{d}\bar{\nu}$ corresponds to the area of the absorption band for a given vibrational mode of a molecular species i and $A_i = \int\sigma_i(\bar{\nu})\mathrm{d}\bar{\nu}$ (cm molecule^{-1}) is the band strength or the integrated absorption coefficient for the particular absorption band that is a constant obtained from literature.

The CH_3OH column densities were calculated from the integrated areas of two absorption bands: the C–O stretch band around 1025 cm^{-1} and the symmetric C–H stretch band around 2828 cm^{-1}, these were then compared and averaged. The C–O stretch was selected because of its high intensity and that it does not overlap with H_2O bands except for the tail of the H_2O libration mode around 760 cm^{-1} (just outside of our spectral range), where a polynomial baseline was subtracted. The C–H stretch band was selected for comparison as its band strength is known to be largely independent of the effects of dilution with H_2O.[25] However, errors in determining the area of the band arise due to the determination of the baseline, as it lies on the red wing of the combined water and methanol O–H stretch. Nevertheless, the column densities determined from each of the bands of methanol were within ±10% of each other and an average of the two values was used for the final column density of CH_3OH for each of our samples.

The H_2O column densities were calculated from the integrated areas of the two most intense bands in our spectral range: the O–H stretch band (around 3270 cm^{-1}) and the O–H bend (around 1670 cm^{-1}). However, it was not possible to directly measure the areas of these bands as they both overlap with CH_3OH absorption features. The band areas were therefore determined by fitting a pure H_2O spectrum to the mixed spectra, subtracting it from the mixed spectrum and examining the residual spectra around the region of the libration mode near the low frequency cut-off of our spectral range, the combination modes (~2200 cm^{-1}) and more specifically in the O–H bending region, as shown in Fig. 1. Due to the strong interactions between CH_3OH and H_2O (discussed later), that give rise to shifts in band positions and changes in width, the residuals around the O–H bending mode region contained both positive and negative components. The fitting was thus iterated and the residuals minimised so that the sum of the positive and negative components in all regions except the O–H stretch where as close to zero as possible. The integrated band areas of the O–H stretch and the O–H bend bands in the fitted pure H_2O spectrum were then used to calculate the H_2O column densities, using linear baselines from 3900 to 2690 cm^{-1} for the O–H stretch and from 1960 to 1060 cm^{-1} for the O–H bend. Errors in the resulting water band areas were between a few % to 10% and the column densities determined from the two bands were found to be within ±5% of each other.

The column densities N_{CH_3OH} and N_{H_2O} were then calculated from eqn (3). The integrated absorption coefficients or the '*A*-values', as they are commonly referred to in the literature, for the four absorption bands were derived from reported values in the literature. *A*-Values of 2.0×10^{-16} cm molecule^{-1} and 1.2×10^{-17} cm molecule^{-1} were used for the O–H stretch (near 3270 cm^{-1}) and the O–H bend (near 1670 cm^{-1}) bands of H_2O respectively.[46] It is to be noted that there is considerable variation in the *A*-values reported[11,25,26,47,48] for the bands of methanol, with little consistent dependence on the mixing medium, within the error limits of up to 30%. We used averaged values of 1.6×10^{-17} cm molecule^{-1} and 5.6×10^{-18} cm molecule^{-1} for the C–O stretch and the symmetric C–H stretch bands of CH_3OH respectively. The methanol column densities calculated using either the C–H stretch, the C–O stretch band or both were well within the errors introduced by the *A*-values. Furthermore, any errors introduced by the *A*-values would only produce a systematic shift in our data and therefore not affect the trends that we observe.

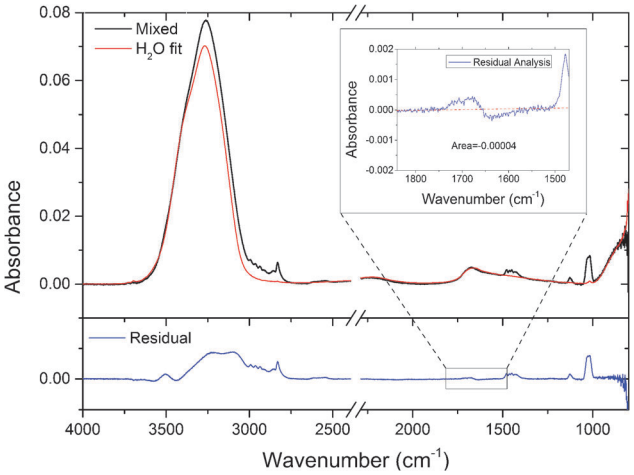

Fig. 1 An example of the fitting process used to determine the H_2O column density. A pure H_2O spectrum is fitted to the mixed spectrum (R = 0.16 in this example) and subtracted such that the residual provides a flat baseline underneath all the CH_3OH features, except the O–H stretch where there is severe overlapping and interaction between CH_3OH and H_2O, and that the sum of the positive and negative components are close to zero in the H_2O bending region (an expanded region is shown in the inset).

In the remainder of this paper we refer to the mixing ratio, R, between CH_3OH and H_2O as a ratio of their column densities, where

$$R = \frac{N_{CH_3OH}}{N_{H_2O}} \quad (4)$$

We have measured the infrared spectra of 18 samples of CH_3OH/H_2O at 30 K, with different relative concentrations as listed in Table 1.

3 Results and discussion

3.1 Comparison between pure and mixed CH_3OH and H_2O amorphous films

The spectra of the mixed CH_3OH and H_2O show considerable changes in the observed band profiles as a function of concentration and specific regions of the spectrum will be discussed in

Table 1 Mixing ratios of samples deposited at 30 K, as determined from the CH_3OH and H_2O column densities, N_{CH_3OH} and N_{H_2O} respectively, calculated from the infrared spectra as described in Section 2.1

Mixing ratio $R = \frac{N_{CH_3OH}}{N_{H_2O}}$	$N_{CH_3OH} \times 10^{16}$ (molec. cm^{-2})	$N_{H_2O} \times 10^{16}$ (molec. cm^{-2})
0.0055 ± 0.0005	0.13 ± 0.01	23.07 ± 1.63
0.14 ± 0.01	3.21 ± 0.17	22.91 ± 1.62
0.16 ± 0.01	3.99 ± 0.21	25.02 ± 1.77
0.22 ± 0.02	5.00 ± 0.26	22.67 ± 1.60
0.38 ± 0.03	8.58 ± 0.43	22.62 ± 1.60
0.52 ± 0.04	7.52 ± 0.37	14.58 ± 1.03
0.62 ± 0.05	9.40 ± 0.46	15.19 ± 1.07
0.67 ± 0.06	10.43 ± 0.51	15.66 ± 1.11
0.74 ± 0.07	6.29 ± 0.33	8.48 ± 0.60
1.00 ± 0.08	7.57 ± 0.38	7.59 ± 0.44
1.14 ± 0.09	7.64 ± 0.39	6.71 ± 0.40
1.24 ± 0.11	7.20 ± 0.36	5.80 ± 0.41
1.48 ± 0.13	8.48 ± 0.42	5.72 ± 0.40
1.64 ± 0.14	8.84 ± 0.43	5.38 ± 0.38
1.78 ± 0.15	13.28 ± 0.64	7.46 ± 0.53
1.90 ± 0.16	12.00 ± 0.56	6.30 ± 0.45
2.31 ± 0.20	9.80 ± 0.47	4.24 ± 0.30
2.83 ± 0.24	11.81 ± 0.56	4.17 ± 0.29
Pure CH_3OH	22.42 ± 0.14	

detail in the following sections with particular focus on the C–O stretch of CH_3OH. However, we will initially briefly compare one example of a mixed CH_3OH and H_2O sample with R = 0.52 with that of pure CH_3OH and H_2O spectra prepared under the same conditions, as shown in Fig. 2, in order to assign the bands (shown in Table 2) and introduce the various regions of the spectrum that will be referred to throughout the remainder of this paper. It is obvious from Fig. 2 that the features in the infrared spectrum of the mixed example sample differ significantly from those of the spectra of the pure constituents. This is clear indication that there is considerable interaction between the CH_3OH and the H_2O molecules within the mixed ice matrix.

The most intense band in the spectrum is due to overlapping O–H stretching modes of CH_3OH (ν_1) and H_2O (ν_1, ν_2) around 3260 cm^{-1}. In the mixed ice this band is visibly broadened and its peak maximum is red-shifted with respect to pure H_2O and blue-shifted with respect to pure CH_3OH. Changes in the frequency of the O–H stretching mode in both CH_3OH and H_2O components are indicative of hydrogen bonding. This band exhibits changes in width and position as a function of R as will be discussed in Section 3.2. The O–H bending band (ν_2) of H_2O that peaks at 1659 cm^{-1} in pure H_2O appears slightly narrowed and blue-shifted in the mixed sample. Blueshifts in the O–H bending mode are indicative of strong hydrogen bonding. A further blue-shift in the presence of CH_3OH might therefore suggest stronger $CH_3OH\cdots H_2O$ hydrogen bonding than $H_2O\cdots H_2O$. In fact $CH_3OH\cdots H_2O$ binding energy is reported to be higher than that for both $H_2O\cdots H_2O$ and $CH_3OH\cdots CH_3OH$.[51]

The C–H stretching region of CH_3OH lies on the red wing of the O–H stretch band between 2700 and 3020 cm^{-1}. There is a slight blue-shift in the symmetric C–H stretch band ($\nu_{3(s)}$) around 2829 cm^{-1} and a shoulder appears around 2853 cm^{-1} that is only present in mixtures with H_2O. It is also interesting to note that the asymmetric C–H stretch region that appears as a broad bumpy feature in pure CH_3OH, exhibits four distinct peaks around 2990, 2960, 2935 and 2910 cm^{-1} in the mixed sample,

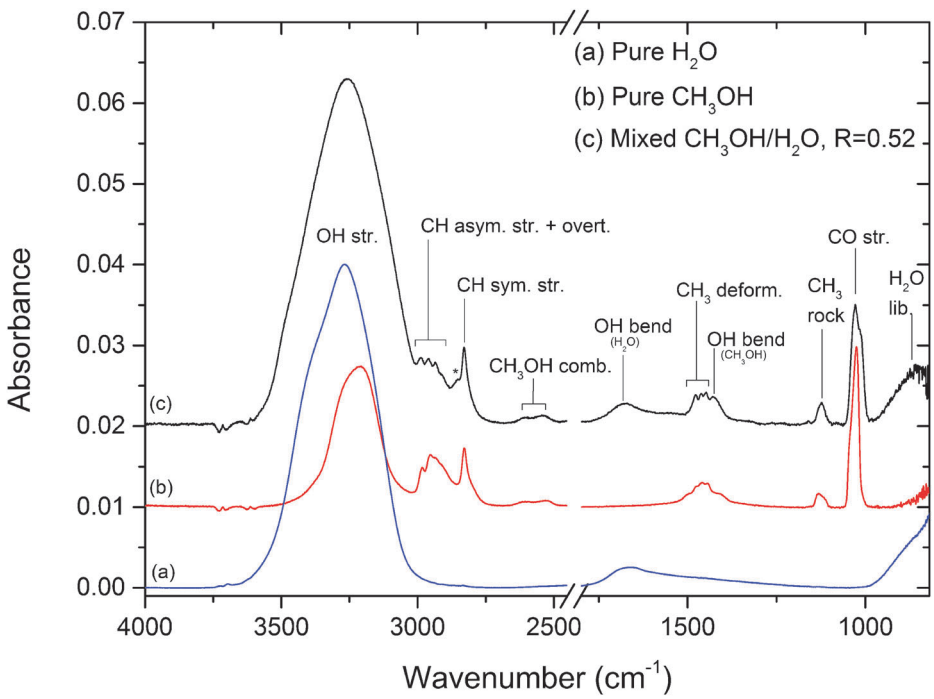

Fig. 2 Comparison between the infrared spectra of (a) pure H_2O, (b) pure CH_3OH and an example of a mixed CH_3OH/H_2O sample with R = 0.52 showing band assignments. The pure H_2O and CH_3OH spectra are normalised to the column densities of H_2O and CH_3OH that constitute the mixed sample.

Table 2 Comparison between band positions of the pure CH_3OH, H_2O and one mixed R = 0.52 sample shown in Fig. 2. Band assignments are from (a) Hagen *et al.*,[49] (b) Hänninen *et al.*[50] and (c) Yukhnevich *et al.*[37] (sh) = shoulder

Molecule	Mode	Assignment	Reference	Pure CH_3OH ($\tilde{\nu}$ cm^{-1})	Pure H_2O ($\tilde{\nu}$ cm^{-1})	Mixed R = 0.52 ($\tilde{\nu}$ cm^{-1})
H_2O	ν_1, ν_3	O–H stretch	a		3272	
	ν_2	O–H bend	a		1659	1673
	$\nu_2 + \nu_L$	Combination	a		2213	2236
CH_3OH	ν_1	O–H stretch	a and b	3208		
	$\nu_{2(a)}$	C–H asym. stretch	a and b	2983		2988
	$\nu_{9(a)}$	C–H asym. stretch	a and b	2953		2960
	$2\delta_a$	CH_3 overtone	c	2932(sh)		2934
	$2\delta_a$	CH_3 overtone	c	2910(sh)		2910
	$\nu_{3(s)}$	C–H sym. stretch	a and b	2828		2829
	$\nu_6 + \nu_8$	Combination	a	2602		2603
	$\nu_6 + \nu_9$	Combination	a	2527		2540
	$\nu_4(\delta_a)$	C–H bend	b and c	1475		1477
	$\nu_{10}(\delta_a)$	C–H bend	b and c	1458		1462
	$\nu_5(\delta_s)$	C–H bend	b and c	1444		1449
	ν_6	O–H bend	a and b	1408(sh)		1427
	ν_7, ν_{11}	CH_3 rock	b	1131, 1117(sh)		1123
	ν_8	C–O stretch	a and b	1025		1027, 1015(sh)
Mixed		Overlapped O–H stretch				3258
		Unassigned				2853

indicating a separation of the two asymmetric stretching modes ($\nu_{2(a)}$ and $\nu_{9(a)}$) and the two overtone bending modes ($2\delta_s$). As with the O–H stretch, the C–H stretch bands exhibit a change in position and width as a function of mixing ratio, R. A more detailed discussion of this region follows in Section 3.3.

The CH_3 bending modes (ν_4, ν_5 and ν_{10}) of CH_3OH lie on the red wing of the H_2O O–H bending band between 1300 and 1550 cm^{-1}. Similarly to the C–H stretching modes, the C–H bending modes overlap and appear as a broad feature in pure CH_3OH, but the four modes become better defined and blue-shift in the mixed samples. Around 1130 cm^{-1}, the CH_3 rocking mode band consists of two broad components (ν_7 and ν_1) in pure CH_3OH, but only a single peak is evident in the mixed sample around 1123 cm^{-1}. The C–O stretch band (ν_8) of CH_3OH appears as a sharp, slightly asymmetric peak around 1027 cm^{-1} in pure CH_3OH. However, in the mixed sample this band is red-shifted and exhibits a low frequency shoulder. The C–O stretch of CH_3OH is very sensitive to the interaction between CH_3OH and H_2O and shows a progressive change in profile as a function of CH_3OH concentration. A detailed analysis of this band follows in Section 3.4.

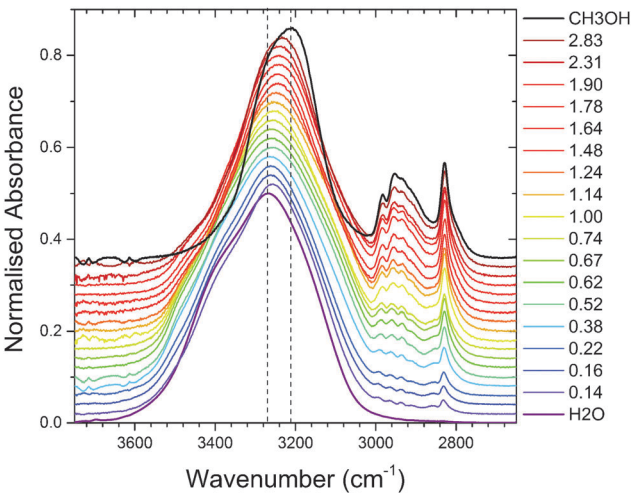

Fig. 3 The O–H stretch and the C–H stretch region of mixed CH_3OH/H_2O samples at 30 K, for different mixing ratios, R. Spectra are normalised to the peak intensity of the O–H stretch band and offset equally by 0.02 for clarity. The dotted lines indicate the positions of the pure CH_3OH and H_2O O–H stretch bands (spectra represented with thicker lines).

3.2 The O–H stretch

The complexity in analysing the O–H stretch band in mixtures of CH_3OH and H_2O lies in the fact that the O–H stretch of CH_3OH and the O–H stretch of H_2O completely overlap. Fig. 3 shows the effect of CH_3OH/H_2O ratio on the O–H stretch band (and the CH_3OH C–H stretching region, which will be discussed separately in Section 3.3). There is a progressive red-shift in the peak position of the combined O–H stretch band from that of pure H_2O at 3268 cm^{-1} to that of pure CH_3OH at 3210 cm^{-1} with increasing R. The position of the peak maximum is plotted as a function of R in Fig. 4 and can be seen to progressively red-shift with increasing R. However the slope of the shift as a function of R changes gradient around R = 0.6.

A certain degree of shifting is expected as the O–H stretch band is composed of the O–H stretching contributions from both species, where the pure components have different band maxima, so as the relative intensity of the CH_3OH and H_2O components change as a function of R, so will the resulting peak position, and the measured peak will lie somewhere between that of pure CH_3OH and H_2O. As expected, therefore the position of the band maxima in the mixtures are always blue-shifted with respect to the pure CH_3OH and red-shifted with respect to pure H_2O band positions. It is intriguing however, looking at Fig. 4 that shows the change in band position as a function of R, that there is clearly an abrupt change in gradient at R = 0.6. So the shift in the composite band

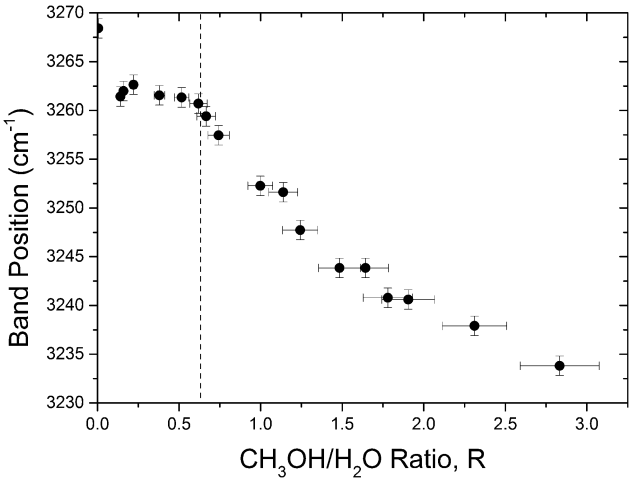

Fig. 4 The O–H stretch peak position of mixed CH_3OH/H_2O samples as a function of mixing ratio, R. There is a clearly a change in gradient around R = 0.6, as highlighted with the dashed vertical line, that is indicative of two different bonding environment regimes.

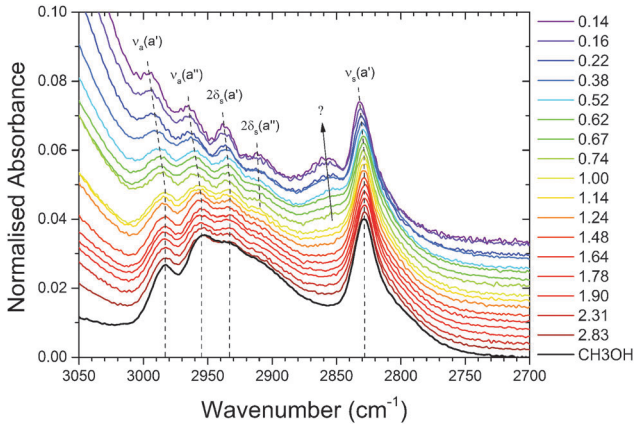

Fig. 5 The C–H stretch region in mixed CH_3OH/H_2O samples at 30 K for different mixing ratios, R. Spectra are normalised to the maximum of the symmetric C–H stretch band (ν_s), offset equally by 0.02 and compared with pure CH_3OH (spectrum indicated with a thicker line). Vertical guides show the evolution of the features with R, clearly showing a blue-shift in the band positions with increasing dilution of CH_3OH in H_2O. A new and yet unassigned feature appears at higher H_2O concentrations (lower R) at around 2858 cm^{-1} (indicated with a vertical arrow). Band assignments are from Yukhnevich *et al.*[37]

maximum position in the mixed samples cannot be accounted for by the 'summation' effect of the pure constituents alone. In fact, looking at Fig. 1 showing an example of a pure H_2O spectrum subtracted from the spectrum of a mixed sample, the O–H stretch region in the residual spectrum does not resemble the O–H stretch of pure CH_3OH after the H_2O O–H stretch band is subtracted. The picture is certainly complicated by the hydrogen bonding interaction between CH_3OH and H_2O. The general red-shift in the O–H stretching frequency of H_2O with the progressive addition of CH_3OH (with increasing R) indicates stronger H_2O proton donating hydrogen bonds as the O–H bond lengthens and weakens, also corroborated by the blue-shift in the H_2O O–H bending mode as hydrogen bonding suppresses the bending mode. However this does not explain the change in gradient around R = 0.6 in Fig. 4. There clearly appears to be a physical change in the way the molecules bond to each other in the mixed samples, with two different regimes apparent below and above R = 0.6. The reason for this will become apparent in the analysis of the C–O stretch band in Section 3.4, henceforth we make no further detailed analysis of the O–H band in this paper.

3.3 The C–H stretch region

There is a progressive blue-shift in the symmetric (ν_a) and asymmetric (ν_s) C–H stretch bands of CH_3OH with increasing dilution in H_2O, as can be seen in Fig. 5, but little to no shifting is observed in the overtone bands ($2\delta_a$). The blue-shift appears to be more pronounced in the asymmetric stretch bands than the symmetric C–H stretch. The band positions in the C–H stretch region are plotted as a function of CH_3OH/H_2O ratio as shown in Fig. 6. It is interesting to note that the onset of the blue-shift in the C–H stretch bands and the appearance of a new band around 2855 cm^{-1} occurs below R = 0.6–0.7. This is consistent with the position where the gradient changes in the O–H stretch position as a function of concentration in Fig. 4, thus supporting the hypothesis that there are two different hydrogen-bonding regimes. Shifts in the C–H stretching frequencies would suggest that they are involved, either directly or indirectly, in bonding.

There are mixed views in the literature about the role of the CH_3OH methyl group in bonding. In some cases it is considered hydrophobic and thus not involved in intermolecular interactions with either neighbouring CH_3OH or H_2O molecules.[30,32,36,52] In fact this appears to be the view held in the astronomy community where the role of the methyl group in intermolecular interactions is generally neglected. While in clusters, thin (monolayer) films and in the gas phase the methyl group shows hydrophobic behaviour, there has also been much discussion in the physical chemistry literature about the so-called 'blue-shifting' hydrogen bonds, with evidence to suggest that the C–H hydrogens in the methyl group of CH_3OH in liquids do indeed take part in bonding[37,38,53–55] and that the weak bonds formed between the methyl hydrogens and an oxygen on the neighbouring CH_3OH or H_2O, are indeed considered to be true hydrogen bonds.[56,57] These bonds are associated with characteristic blue-shifts in the C–H stretching frequency. Therefore, not unlike the liquid phase, in the bulk amorphous solid it is highly likely that the methyl group does indeed participate in hydrogen bonding. Thus the increasing blue-shift in the C–H bands below R = 0.6–0.7 that we see in Fig. 5 and 6 strongly suggest that the methyl group begins to form hydrogen bonds, most likely with H_2O molecules due to higher H_2O concentrations at low R. Interestingly this is also around the mixing ratio where we hypothesise the change in the bonding environment observed in Fig. 4 showing the variation in the O–H stretch position as a function of R. The splitting of the C–H stretch region in the mixed samples into four distinct bands compared to that of the less defined region in pure CH_3OH in fact suggests that only one CH_3 hydrogen

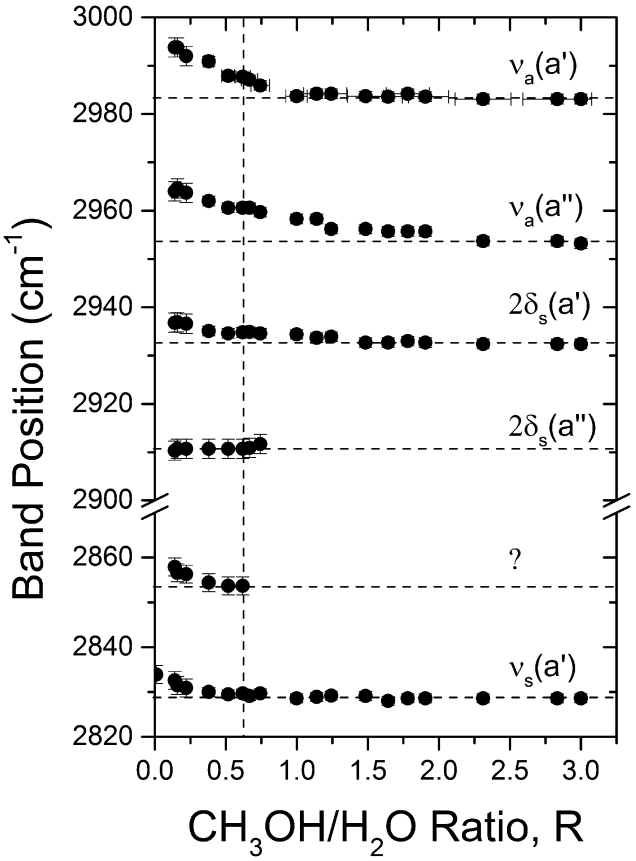

Fig. 6 Band positions in the C–H stretch region of mixed CH_3OH/H_2O samples as a function of mixing ratio, R, clearly showing a more pronounced blue-shift in the asymmetric bands ν_a, and asymmetric ν_a, stretch bands and a slight blue-shift in one of the $2\delta_a$ overtone bands. A new yet unassigned band (?) appears below R = 0.6. Band assignments are from Yukhnevich *et al.*[37]

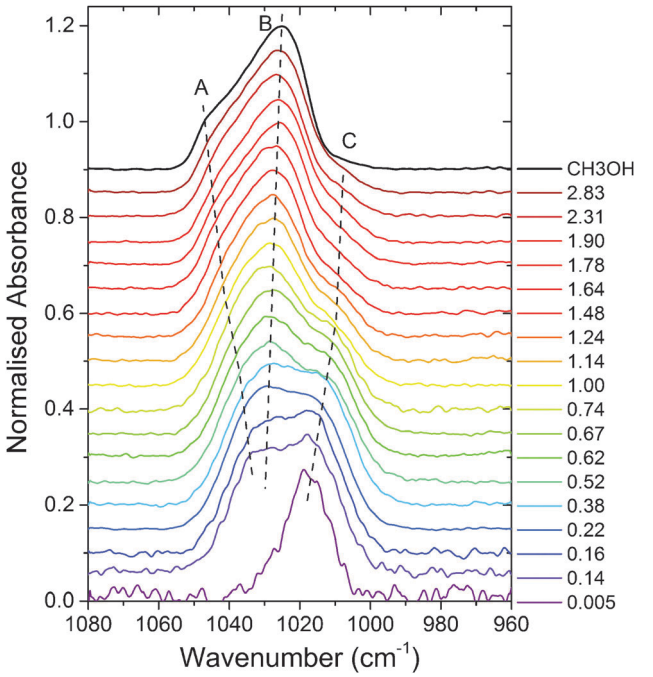

Fig. 7 Evolution in the C–O stretching band profile with varying CH_3OH/H_2O concentration, compared with that of pure CH_3OH. This band clearly consists of three sub-components indicated with dashed lines and labelled A–C, with the 'red' component, C, that is uniquely present in the presence of H_2O.

participates in a hydrogen bond.[37] This may also explain the comparatively smaller blue-shift of the symmetric stretch band (ν_s) compared to the asymmetric bands (ν_a). In order to fully understand the nature of interaction between CH_3OH and H_2O, especially at low CH_3OH concentrations, we focus our attention on the C–O stretch of CH_3OH in the following section. The C–O bond is the bridge between the CH_3 and the OH ends of the CH_3OH molecule and is therefore sensitive to changes in electron density resulting from hydrogen bonding, and will thus provide further insight into the nature of hydrogen bonding as a function of R.

3.4 The C–O stretch of CH_3OH

3.4.1 C–O band spectral features. Fig. 7 shows the spectra of the C–O stretch of CH_3OH for different mixing ratios, R. In pure CH_3OH this band is asymmetric, peaking at around 1025 cm^{-1}. The asymmetry of the band suggests the presence of sub-components. This becomes more apparent as the mixing ratio, R, is altered (as seen in Fig. 7), suggesting that the subcomponents of the C–O stretching band are also related to the broader global changes occurring in the ice bonding and structure, and is indicative that, as we previously hypothesised, the C–O band is a reliable measure of the hydrogen bonding network in mixed CH_3OH/H_2O ices.

Notably, compared to the band profile of pure CH_3OH, a red shoulder appears in mixtures containing H_2O, that grows in intensity with increasing H_2O concentration (decreasing R). In the very dilute CH_3OH sample (R = 0.005), this 'red component', peaking at 1017 cm^{-1}, appears to be the dominant feature. Shifts of the C–O stretch as a function of concentration have been reported in literature, for example, Schutte *et al.* reported C–O stretch peak positions of 1018 and 1028 cm^{-1} for R = 0.05 and R = 0.67 respectively, in CH_3OH/H_2O mixtures deposited at 10 K.[22] The presence of subcomponents have also been reported, for example Ahmed *et al.* report a shift from 1015 cm^{-1} to 1022 cm^{-1} in going from 0.1 to 0.9 mole fraction in liquid mixtures of CH_3OH/H_2O and attributed this to the presence of four sub-components at (i) 1060, (ii) 1023, (iii) 1010 and (iv) 1000 cm^{-1}, assigned to different combinations of hydrogen bonding within the liquid: (i) CH_3OH H bonded with either H_2O or CH_3OH, (ii) both O and H simultaneously bonded to two CH_3OH molecules, (iii) both O and H simultaneously bonded to two H_2O molecules and (iv) with CH_3OH O bonded to either H_2O or CH_3OH, respectively.[32] Similarly, Bahr *et al.* have reported the presence of three components at (i) 1048, (ii) 1034 and (iii) 1015 cm^{-1} in the RAIRS spectra of the C–O stretch of CH_3OH adsorbed onto amorphous solid water at 121 K.[51] The authors assign the bands to (i) multilayer CH_3OHC-CH_3OH bonds, (ii) interaction of CH_3OH with the H_2O surface and (iii) the interaction of CH_3OH with both the H_2O surface and the first complete layer of CH_3OH, respectively.

In order to investigate the apparent subcomponents in our data and understand their physical significance, we have fitted the C–O stretching band with a linear combination of Gaussian functions. Gaussian functions were found to provide the best fits to the band profile over Lorentzian or Voight functions. Indeed the Gaussian oscillator model is appropriate for absorption bands in strongly bonding disordered amorphous solids within which the intermolecular interactions give rise to a random distribution of bond lengths and angles. Thus each vibrational band is composed of a normal distribution of oscillators centred around an average peak frequency. Three Gaussians were fitted to the C–O stretch band of CH_3OH, one representing each clear component: two that are present in pure CH_3OH and a third that fits the red shoulder in the mixed samples. It was difficult to fit three components at low R values where the peak positions of the two 'pure CH_3OH' components appear to converge, as can be seen in Fig. 7 (dashed lines A and B). In these cases both a two- and a three-component fit were computed, and although the general results were commensurate with each other, in all cases the errors and the χ-squared values were lower in the three-component fit as can be seen in the example shown in Fig. 8 for $R = 0.67$. Therefore for the remainder of this paper we discuss the C–O stretch band in terms of three sub-components, a 'red', 'blue' and 'middle' component.

The results of the Gaussian fits confirm that the C–O stretch of CH_3OH mixed in H_2O comprises of the three sub-components: a 'blue' component that shifts from 1037 cm^{-1} to 1041 cm^{-1}, a 'middle' component that shifts from 1029 cm^{-1} to 1025 cm^{-1}, and a 'red' component that shifts from 1017 cm^{-1} to 1007 cm^{-1} with increasing R. Fig. 9 clearly shows the greatest variability in peak position occurs in the red component, which is red-shifted with increasing R indicating that the C–O bond is weakening in the associated ice environment as the CH_3OH concentration increases. Conversely, the blue and middle components show significantly less positional alteration, but diametrically opposite behaviour, with the middle (green) component slightly red-shifting with increasing R whilst the blue component is increasingly blue-shifted, indicating strengthening of the electron density in the C–O bond in this environment.

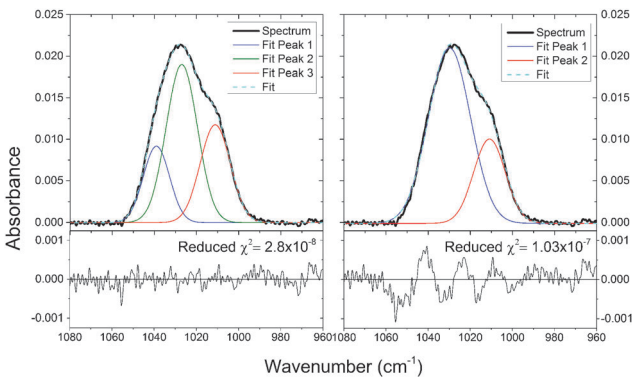

Fig. 8 An example of three and two Gaussian fits to the C–O stretch of CH_3OH for a sample with $CH_3OH/H_2O = 0.67$. Corresponding residuals are shown below each graph together with the respective reduced χ^2 values from the fit.

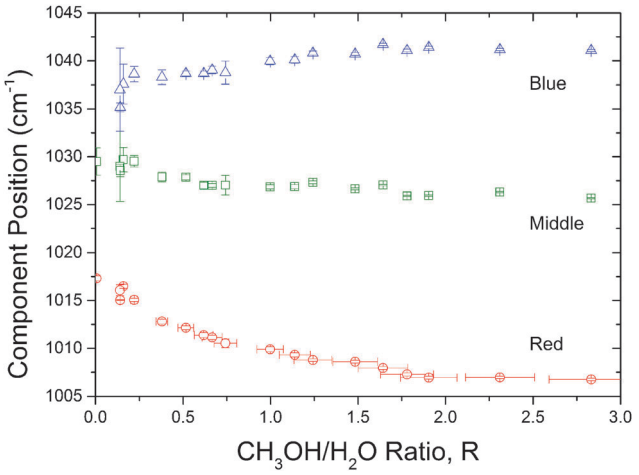

Fig. 9 The change in the peak position of three components, as derived from the Gaussian fits, of the C–O stretch band of CH_3OH as a function of CH_3OH/H_2O ratio.

It is obvious from Fig. 7 that not only the sub-component positions but also their intensities are changing with R. Therefore it may be more informative to investigate how the area of the fitted components, relative to the total band area, change as a function of R. This is illustrated in Fig. 10. It can clearly be seen that, within the error bars, the relative area of the blue component remains independent of the CH_3OH concentration and constitutes about 21% of the total band area. However, the relative area of the red component decreases as the relative area of the middle component increases, crossing over around $R = 0.5$ (indicated with a dashed line in Fig. 10). In fact, plotting the normalised area of the middle component against the normalised area of the red component, (shown in Fig. 11), shows that they are inversely related, yielding a linear fit with a gradient that is very near to 1. Incidentally, at $R = 0.5$ stoichiometry dictates that there are two H_2O molecules to every

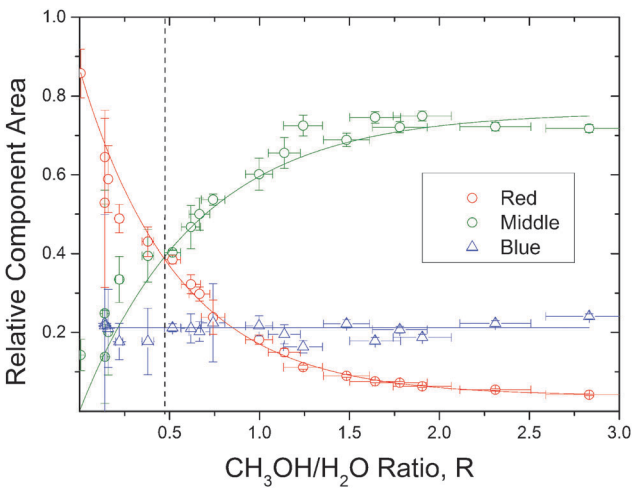

Fig. 10 The variation of the band areas (relative to the total band area) of the three components of the C–O stretch band of CH_3OH, as derived from the Gaussian fits, as a function of CH_3OH/H_2O ratio, R.

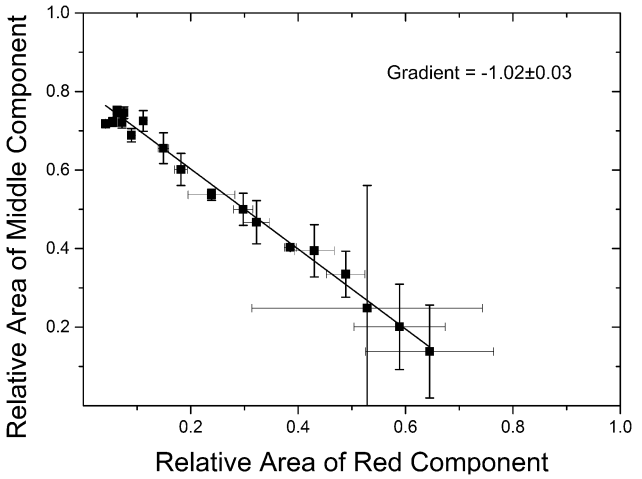

Fig. 11 Relative area of the middle component *versus* the relative area of the red component, showing inverse linear correlation between the two components. The slope of the fitted line is −1.02 ± 0.03 and a Pearson's correlation coefficient of −0.99378.

CH_3OH molecule where the red and middle components cross and it would appear that the environment that gives rise to the middle component for $R > 0.5$ is directly replaced with an environment that gives rise to the red component for $R < 0.5$. Therefore, it would appear that for every ice mixture there are at least two (and sometimes three) bonding environments, the question is what are they? We attempt to answer this in the next section.

3.4.2 CH_3OH as a proton donor/acceptor. Clearly the red component of the C–O stretch band of CH_3OH is only present in the presence of H_2O. But what structural orientations explain the blue and middle C–O stretch spectral features? Experimental and computational studies of CH_3OH dimers have shown that the infrared spectrum of the C–O stretch is comprised of two peaks, one red-shifted (by −6.8 cm^{-1}) and one blue-shifted (by +18.5 cm^{-1}) from the C–O stretching mode of the monomer around 1033.5 cm^{-1}.[58] These peaks have been attributed to the CH_3OH molecule acting as a proton acceptor (PA) and a proton donor (PD) respectively. When the molecule acts as a PA *via* the lone pairs of electrons on the O atom, the attractive hydrogen bond draws the electron density away from the C–O bond, resulting in an elongation of the bond and hence a red-shift in the vibrational frequency. Conversely, when the molecule acts as a PD, the coupling to the O–H bond results in a shortening in the C–O bond length, hence a blue-shift in the vibrational frequency. In our data, the shift of around +4 to +8 cm^{-1} in the blue component position and around −5 to −9 cm^{-1} in the middle component compared to the C–O stretching frequency of a free CH_3OH molecule could therefore be regarded as CH_3OH molecules acting as PA and PD respectively within the amorphous ice matrix. While splitting into distinct components within a solid requires symmetric coupling and long range order, such as in crystalline solids, within the bulk of an amorphous solid some molecules will simultaneously act as both PA and PD and some incomplete bonding is expected with free dangling–H bonds and un-bonded O lone pairs, providing a range of C–O stretch oscillator strengths, some short range order is expected essentially forming short chains, branches and cyclic structures. Nevertheless, what we observe in our spectra is the sum of the cooperative effects within the statistical distribution of bonding and non-bonding environments clearly giving rise to two broad components that can be distinguished, based on shifts in the vibrational frequency, into a blue-shifted PD dominated environment (blue component) and a red-shifted PA dominated environment (middle component).

Now let us consider what happens when CH_3OH is diluted in H_2O. Both the middle and the blue components of the C–O stretch are present as R decreases, however as seen in Fig. 10, the blue component area remains more or less constant relative to the total C–O stretch band area. Therefore, it would appear that the presence of H_2O environment has little effect on the CH_3OH PD hydrogen bonds. It has been reported in literature[33–35,39,58] that gas phase and matrix isolated hetero-dimers of CH_3OH and H_2O preferentially and exclusively bond with the CH_3OH acting as a PA and the H_2O as PD. Within an amorphous solid where a random arrangement of molecules and hydrogen bonded configurations are likely, it is still possible that during deposition there is preferential adsorption of CH_3OH and H_2O in the $CH_3OH(PA)HH_2O(PD)$ arrangement. In fact, the observed blue-shift in the O–H bending mode and a red-shift in the O–H stretching mode of H_2O with increasing CH_3OH concentration (Fig. 4) is also consistent with this picture. It is also interesting to note that in this arrangement, with CH_3OH acting as a PA when bonded to H_2O acting as a PD, no significant change in the O–H bond length of CH_3OH is reported.[33,58] Therefore with this picture in mind, that CH_3OH molecules are most likely to act as a PA to H_2O with increasing H_2O concentration (decreasing R), it would stand to reason that the blue PD C–O stretch component of CH_3OH would thus remain unaffected, as our results show.

While the blue C–O stretch component (corresponding to a PD CH_3OH) appears to be constant, the middle component (corresponding to a PA CH_3OH environment) appears to decrease with increased H_2O concentration (decreasing R) and be directly replaced by the red component (Fig. 11), thus suggesting that the latter must also relate to a PA environment and be directly associated with H_2O concentration. However, *ab initio* calculations show that there is only a small difference between the relative binding strength of the $CH_3OH(PA)\cdots CH_3OH(PD)$ and the $CH_3OH(PA)\cdots H_2O(PD)$ hydrogen bonds.[39] Thus replacing a CH_3OH donor molecule with a H_2O donor molecule at the PA site of a CH_3OH molecule is not sufficient to produce the considerable red-shift in the C–O stretching frequency we observe in the red component (between −17 and −26 cm^{-1} relative to the free CH_3OH). So what is the origin of the red component?

It is clear that the red component of the C–O stretch band of methanol is indicative of the presence of H_2O as it is only seen in the spectra when H_2O is present in the matrix. Therefore, in order to distinguish the behaviour of this 'water' component and its relationship with the 'methanol' components, we have plotted the sum of the blue and middle components

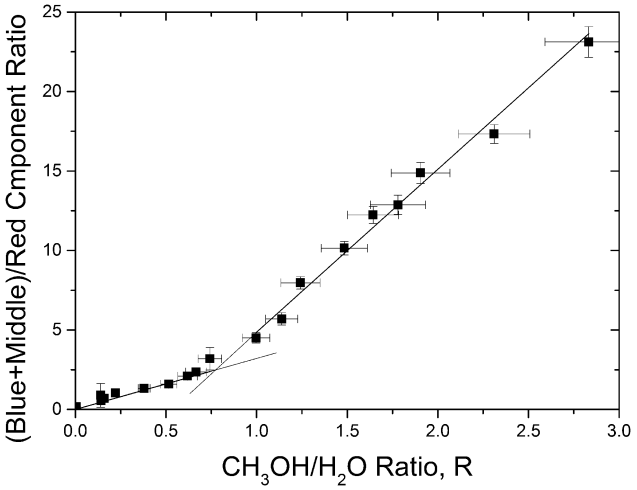

Fig. 12 The ratio of the pure CH_3OH components (blue and middle) to the red component (seen only in mixtures with H_2O) as a function of CH_3OH/H_2O ratio, R. The graph shows a linear relationship below $R = 0.5$, with a gradient of 3.2 ± 0.1, and above $R = 1$, with a gradient of 10.2 ± 0.5. The linear relationship confirms that the red component of the C–O stretch of CH_3OH is directly related to the presence of H_2O.

(the only components present in pure CH_3OH) as a ratio of the red component (present exclusively in the presence of H_2O) against CH_3OH/H_2O mixing ratio, as shown in Fig. 12. The graph shows a linear relationship below $R = 0.5$, with a gradient of 3.2 ± 0.1, and above $R = 1$, with a gradient of 10.2 ± 0.5. Indeed, the linear relationship confirms that the red component of the C–O stretch of CH_3OH is directly related to the presence of H_2O. Stoichiometrically, the turning point occurs over a range of R, going from an environment where there are two H_2O molecules to every CH_3OH ($R = 0.5$) to an environment where there is one H_2O to every CH_3OH ($R = 1$). This suggests that the red component is related to the hydrogen bonded molecular coordination number.

In crystalline H_2O, molecules are able to arrange in tetrahedral structures, forming hydrogen bonds with four nearest neighbours – two PA bonds at the two lone pairs of electrons on the oxygen atom and two PD bonds with the O–H groups. In contrast, in pure crystalline CH_3OH the molecules arrange in linear chains as each CH_3OH molecule forms hydrogen bonds with just two nearest neighbours – a PA bond with only one lone pair of electrons on the oxygen atom and one PD bond with the O–H group. In an amorphous solid, however, there is no long-range order that is not too dissimilar to that of the liquid phase. In the less ordered structure in liquid CH_3OH, the molecules arrange in chains, with bi-coordinated hydrogen bonds being the most probable, and the less probable single and tri-coordinated hydrogen bonds forming terminated chains and branches respectively. Thus in a mixture of CH_3OH and H_2O, we would expect a mixture of different hydrogen bond coordination numbers ranging from 1 to 3. In fact, computational studies have shown that the mean dipole moment of the CH_3OH molecule depends on the number of hydrogen bonds the molecule makes with its nearest neighbours and that the dipole moment increases with increasing number of hydrogen bonds, suggesting substantial rearrangement of the molecular electron density.[38] The authors point out that the observed trend in liquid CH_3OH closely resembles that of liquid H_2O. Hence the correlation between H_2O concentration with the relative area of the 'red' component below $R = 0.5$, together with the large red-shift in frequency in the C–O stretch, that is associated with a PA hydrogen bond, would seem to suggest that CH_3OH molecules are forming more than one PA bond with the H_2O molecules – similar to the two PA bonds that H_2O molecules make with the two lone pairs of electrons on the oxygen atom.

An experimental and computational study carried out on the adsorption of a single CH_3OH molecule on H_2O clusters[58] has shown that a CH_3OH molecule binds to the H_2O cluster and simultaneously acts as a PA and a PD (as would be expected of most molecules in the bulk of a solid) in a cyclic structure. A particularly interesting result of their experiment is that the CH_3OH molecule forms a third hydrogen bond with another H_2O, using the second lone pairs of electrons on the oxygen atom. The CH_3OH molecule thus simultaneously acts as a PA to two H_2O molecules. Buck *et al.* report that empirical calculations show that this additional interaction causes a further red-shift in the C–O stretching frequency corroborates our hypothesis about the origin of the red component in our data: a CH_3OH molecule acting as a double PA to two PD H_2O molecules. Referring back to Fig. 12, the gradual change in gradient in the graph occurs between $R = 1$ and $R = 0.5$ a region from where there is one H_2O to every CH_3OH to where there are two H_2O molecules to every CH_3OH. The constant gradient below $R = 0.5$ (more than two H_2O molecules per CH_3OH molecule), is where the most probable arrangement is one where each CH_3OH acts as a double PA to two H_2O molecules. The constant gradient above $R = 1$ (less than one H_2O molecule per CH_3OH), is where the most probable arrangement is one where CH_3OH acts as a PA to either one H_2O or a CH_3OH molecule. From Fig. 10 it can be seen that the middle component reaches saturation around $R = 2$, where there are two CH_3OH molecules to every H_2O molecule.

3.4.3 Bringing evidence together from the O–H, C–H and C–O stretch regions. The sub-components in the C–O stretch band of CH_3OH clearly indicate that there is preferential bonding between CH_3OH and H_2O, and that $CH_3OH(PA)\cdots HH_2O(PD)$ is the preferred arrangement, even in vapour deposited samples at 30 K. Furthermore, the mixing between the two species in the amorphous solid appears to be inhomogeneous. This is evidenced by the presence of the red component even at high R. For example in mixtures above $R = 1$, where there is less than one H_2O molecule for every CH_3OH molecule, the presence of the red component indicates that for some CH_3OH molecules there are $2H_2O$ molecules hydrogen bonded to them in a $CH_3OH(2PA)\cdots 2H_2O(PD)$ arrangement that gives rise to the red component in the C–O stretch profile. In fact this behaviour is similar to that of liquid mixtures where evidence of clustering and inhomogeneity have been reported.[59–61] Monte Carlo simulations of CH_3OH/H_2O mixtures have shown two distinct regimes

in the behaviour of the hydrogen bonded network that are related to a change from a percolating regime (below R = 1) to a non-percolating regime.[60] It is interesting to note that in our case this is linked to the bonding preference between the molecules as they adsorb during sample growth, as they are unlikely to rearrange at 30 K, unlike the dynamic structure of hydrogen bonded liquids. This is consistently evident in the global structure of the amorphous solid *via* the profiles of the C–O, C–H and the O–H stretch modes as a function of R.

It has been reported that a red-shift in the C–O stretching frequency is also expected during the formation of a hydrogen bond with a methyl group due to intramolecular charge redistribution.[55] The weak hydrogen bond formed between one of the hydrogen atoms in the methyl group of CH_3OH and a lone pair of electrons on a neighbouring H_2O molecule is accompanied by a weak intermolecular orbital interaction between the proton accepting lone pair and a C–H (σ^*) antibonding orbital. This is thought to result in an increase in the occupancy of the C–O σ^* antibonding orbital corresponding to weakening and elongation of the C–O bond and hence an observed red-shift in the C–O stretching frequency. Consequently there is an intramolecular charge transfer whereby a decrease in the in the orbital interaction between the lone pairs of electrons on the CH_3OH oxygen atom and the C–H σ^* antibonding orbital occurs, which may explain the strengthening and shortening of the C–H bond and hence the observed blue-shift in the asymmetric C–H stretching frequency. Turning this around, Keefe and Istvankova[55] suggest that the blue-shifts in C–H stretching modes could also be due to CH_3OH acting as a PA *via* a lone pair of electrons on the oxygen atom. In this case there is also a decrease in the intramolecular orbital interaction between the oxygen lone pair and the C–H σ^* antibonding orbital as the occupancy in the CH_3OH lone pair decreases during PA hydrogen bond formation. This results in a subsequent decrease in the occupancy of the C–H σ^* antibonding orbital and hence a strengthening, shortening and corresponding blue-shift in the C–H stretching frequency. So how would 2PA bonds on the O atom affect the C–H stretch region? In either case, in our experiments we observe both a blue-shift in the C–H stretching modes and the presence of the red-shifted red component in the C–O stretch mode, both consistent with each other. It is interesting to note that the onset of blue-shifting in the C–H stretching frequency in Fig. 6 is concurrent with the change in the slope in Fig. 12 and also with the change in the slope of the O–H band position in Fig. 4, all around R = 0.6–0.75. Furthermore, a new band that appears and grows in intensity below R = 0.6 in the C–H stretching region (Fig. 5 and 6) may also be related to the red C–O stretch component. With the C–O bond linking the CH_3 and the OH ends of the CH_3OH molecule there is clearly a cooperative effect between intermolecular interactions *via* the CH_3 hydrogens, the double PA oxygen lone pairs and PD O–H hydrogen resulting in significant intramolecular charge redistribution. These effects are concurrent across the different regions of the spectrum with a clear change in the bonding regime occurring below R = 0.6–0.7. At high H_2O concentrations such boding conformations must therefore become sterically favourable within the amorphous solid.

4 Conclusions

We have carried out a detailed systematic study of the infrared spectroscopy of mixtures of CH_3OH and H_2O at 30 K as a function of concentration. It is clear that CH_3OH and H_2O interact strongly within the solid matrix and that the nature of their interaction is strongly dependent on the CH_3OH/H_2O mixing ratio, R. Evidence from the O–H and C–H stretch band positions and detailed analysis of the sub-components of the C–O stretch band clearly indicate that there is a dramatic change in molecular coordination in the mixed hydrogen bonding network with two distinct regimes evident below and above R = 0.6–0.7.

Detailed analysis of the C–O stretch band reveals that it consists of three sub-components in the mixed samples, with a 'red' component that is only present with H_2O. The origin of the 'blue' and the 'middle' components are assigned to environments within the ice matrix in which dominant interactions involve CH_3OH hydroxyl groups as proton donors and acceptors respectively. The 'red' component has been assigned to the CH_3OH molecules in an environment where the molecules can act as double proton acceptors to two H_2O molecules *via* both the lone pairs of electrons on the oxygen atom. The presence of the 'red' component at greater R might also suggest inhomogeneity in the mixing between CH_3OH and H_2O. There is evidence that there is preferential hydrogen bonding of the CH_3OH molecule as a proton acceptor to proton donating H_2O molecules as confirmed by direct correlation between the 'middle' and the 'red' components in the C–O stretch as a function of mixing ratio and a constant blue PD component.

Blueshifts in the C–H stretch positions were observed at mixing ratios below R = 0.6–0.7 suggesting that the methyl group also participates in hydrogen bonding at low CH_3OH concentrations. This is the ratio where we also observe a change in the hydrogen bonding behaviour, with the formation of higher coordinated bonds. It is thus expected that in the regime below R = 0.6–0.7 the solid consists of more branched and cyclic structures with both the O–H and the CH_3 groups in CH_3OH participating in hydrogen bonding, whereas more chains are expected above R = 0.7 and that the solid amorphous mixture resembles the structure of liquid mixtures.

Our results demonstrate that not only does the C–O stretch of CH_3OH provide us with insight into the hydrogen bonding nature and the structure of CH_3OH/H_2O condensed mixtures at 30 K, as a function of mixing ratio, but that it can also be used for the interpretation of observational spectra. The high sensitivity of the C–O stretch band profile on the $CH_3OH\cdots H_2O$ hydrogen bonding environment makes it an ideal candidate to infer spectroscopically whether CH_3OH and H_2O ices exist in segregated or mixed environments in the interstellar medium and on planetary bodies. Furthermore, the three clearly defined components in condensed ices may allow observational astronomers, through the inspection of this band, to determine the degree of mixing, and thus constrain the CH_3OH/H_2O component whilst simultaneously fitting other regions of the spectrum.[27] Though there is still considerable work required to fully understand the nature of

interactions that gives rise to the C–O stretch components, for example as a function deposition temperature, deposition rate and film thickness as well as the effects of thermal and energetic processing, such work would also aid in the interpretation of the physical and chemical environment in which H_2O and CH_3OH ices are formed and exist in interstellar and planetary environments.

Acknowledgements

AD acknowledges the receipt of a Daphne Jackson Fellowship co-sponsored by STFC and the Open University.

References

1 J. E. Chiar, *Planetary and Interstellar Processes Relevant to the Origins of Life*, Springer, 1997, pp. 79–100.
2 J. M. Greenberg, *Astron. Astrophys.*, 1998, **330**, 375–380.
3 P. Ehrenfreund and W. Schutte, *Adv. Space Res.*, 2000, **25**, 2177–2188.
4 D. Whittet, A. Cook, E. Herbst, J. Chiar and S. Shenoy, *Astrophys. J.*, 2011, **742**, 28.
5 D. Bockelée-Morvan, J. Crovisier, P. Colom and D. Despois, *Astron. Astrophys.*, 1994, **287**, 647–665.
6 N. Biver, D. Bockelée-Morvan, J. Crovisier, P. Colom, F. Henry, R. Moreno, G. Paubert, D. Despois and D. C. Lis, *Cometary Science after Hale-Bopp*, Springer, 2002, pp. 323–333.
7 I. Wright, S. Sheridan, S. Barber, G. Morgan, D. Andrews and A. Morse, *Science*, 2015, **349**, aab0673.
8 N. Biver, D. Bockelée-Morvan, J. Crovisier, P. Colom, F. Henry, R. Moreno, G. Paubert, D. Despois and D. C. Lis, *The Solar System Beyond Neptune*, University of Arizona Press, Tucson, 2008, pp. 143–160.
9 F. Merlin, M. Barucci, C. de Bergh, S. Fornasier, A. Doressoundiram, D. Perna and S. Protopapa, *Icarus*, 2010, **208**, 945–954.
10 C. Dalle Ore, M. Barucci, D. Cruikshank and J. Emery, Asteroids, Comets, Meteors 2014. Proceedings of the conference held 30 June–4 July, 2014 in Helsinki, Finland, ed. K. Muinonen, *et al.*, 2014, p. 398.
11 R. J. A. Grim, F. Baas, J. M. Greenberg, T. R. Geballe and W. Schutte, *Astron. Astrophys.*, 1991, **243**, 473–477.
12 E. Dartois, W. Schutte, T. Geballe, K. Demyk, P. Ehrenfreund and L. d'Hendecourt, *Astron. Astrophys.*, 1999, **342**, L32–L35.
13 K. M. Pontoppidan, E. Dartois, E. F. van Dishoeck, W.-F. Thi and L. d'Hendecourt, *Astron. Astrophys.*, 2003, **404**, L17–L20.
14 K. Pontoppidan, E. Van Dishoeck and E. Dartois, *Astron. Astrophys.*, 2004, **426**, 925–940.
15 A. Tielens and W. Hagen, *Astron. Astrophys.*, 1982, **114**, 245–260.
16 N. Watanabe and A. Kouchi, *Astrophys. J., Lett.*, 2002, **571**, L173.
17 D. E. Woon, *Astrophys. J.*, 2002, **569**, 541.
18 N. Watanabe, A. Nagaoka, T. Shiraki and A. Kouchi, *Astrophys. J.*, 2004, **616**, 638.
19 H. Hidaka, N. Watanabe, T. Shiraki, A. Nagaoka and A. Kouchi, *Astrophys. J.*, 2004, **614**, 1124.
20 G. Fuchs, H. Cuppen, S. Ioppolo, C. Romanzin, S. Bisschop, S. Andersson, E. van Dishoeck and H. Linnartz, *Astron. Astrophys.*, 2009, **505**, 629–639.
21 S. Bottinelli, A. A. Boogert, J. Bouwman, M. Beckwith, E. F. Van Dishoeck, K. I. Öberg, K. M. Pontoppidan, H. Linnartz, G. A. Blake and N. J. Evans II, *et al.*, *Astrophys. J.*, 2010, **718**, 1100.
22 W. Schutte, A. Tielens and S. Sandford, *Astrophys. J.*, 1991, **382**, 523–529.
23 S. A. Sandford and L. J. Allamandola, *Astrophys. J.*, 1993, **417**, 815–825.
24 P. Ehrenfreund, O. Kerkhof, W. Schutte, A. Boogert, P. Gerakines, E. Dartois, L. d'Hendecourt, A. Tielens, E. Van Dishoeck and D. Whittet, *Astron. Astrophys.*, 1999, **350**, 240–253.
25 O. Kerkhof, W. A. Schutte and P. Ehrenfreund, *Astron. Astrophys.*, 1999, **346**, 990–994.
26 M. E. Palumbo, A. C. Castorina and G. Strazzulla, *Astron. Astrophys.*, 1999, **342**, 551–562.
27 A. Suutarinen, A. Dawes, H. Cuppen, K. Isokoski, H. Linnartz, J. Noble and H. Fraser, *Mon. Not. R. Astron. Soc.*, 2015, submitted.
28 Y. Hu, H. Fu and E. Bernstein, *J. Chem. Phys.*, 2006, **125**, 154306.
29 D. S. Bulgarevich, K. Otake, T. Sako, T. Sugeta, Y. Takebayashi, C. Kamizawa, D. Shintani, A. Negishi and C. Tsurumi, *J. Chem. Phys.*, 2002, **116**, 1995–2003.
30 W.-T. Liu, L. Zhang and Y. Shen, *J. Chem. Phys.*, 2006, **125**, 144711.
31 G. Georgiev, K. Vasilev and K. Gyamchev, *Bulg. J. Phys.*, 2007, **34**, 103–107.
32 M. K. Ahmed, S. Ali and E. Wojcik, *Spectrosc. Lett.*, 2012, **45**, 420–423.
33 N. Bakkas, Y. Bouteiller, A. Loutellier, J. P. Perchard and S. Racine, *J. Chem. Phys.*, 1993, **99**, 3335–3342.
34 N. Bakkas, Y. Bouteiller, A. Loutellier, J. P. Perchard and S. Racine, *Chem. Phys. Lett.*, 1995, **232**, 90–98.
35 P. A. Stockman, G. A. Blake, F. J. Lovas and R. D. Suenram, *J. Chem. Phys.*, 1997, **107**, 3782–3790.
36 A. Laaksonen, P. Kusalik and I. Svishchev, *J. Phys. Chem. A*, 1997, **101**, 5910–5918.
37 G. Yukhnevich and E. Tarakanova, *J. Mol. Struct.*, 1998, **447**, 257–261.
38 M. Pagliai, G. Cardini, R. Righini and V. Schettino, *J. Chem. Phys.*, 2003, **119**, 6655–6662.
39 E. E. Fileti, P. Chaudhuri and S. Canuto, *Chem. Phys. Lett.*, 2004, **400**, 494–499.
40 S. L. Boyd and R. J. Boyd, *J. Chem. Theory Comput.*, 2007, **3**, 54–61.
41 P. A. Golubkov, J. C. Wu and P. Ren, *Phys. Chem. Chem. Phys.*, 2008, **10**, 2050–2057.
42 I. Bakó, T. Megyes, S. Bálint, T. Grósz and V. Chihaia, *Phys. Chem. Chem. Phys.*, 2008, **10**, 5004–5011.
43 K.-i. Suhara, A. Fujii, K. Mizuse, N. Mikami and J.-L. Kuo, *J. Chem. Phys.*, 2007, **126**, 194306.
44 A. Mandal, M. Prakash, R. M. Kumar, R. Parthasarathi and V. Subramanian, *J. Phys. Chem.*, 2010, **114**, 2250–2258.

45 C. Skinner, A. Tielens, M. Barlow and K. Justtanont, *Astrophys. J.*, 1992, **399**, L79–L82.
46 P. A. Gerakines, W. A. Schutte, J. M. Greenberg and E. F. van Dishoeck, *Astron. Astrophys.*, 1995, **296**, 810.
47 L. B. d'Hendecourt and L. J. Allamandola, *Astron. Astrophys., Suppl. Ser.*, 1986, **64**, 453–467.
48 D. M. Hudgins, S. A. Sandford, L. J. Allamandola and A. G. G. M. Tielens, *Astrophys. J., Suppl. Ser.*, 1993, **86**, 713–870.
49 W. Hagen, A. Tielens and J. Greenberg, *Astron. Astrophys., Suppl. Ser.*, 1983, **51**, 389–416.
50 V. Hänninen and L. Halonen, *Mol. Phys.*, 2003, **101**, 2907–2916.
51 S. Bahr, C. Toubin and V. Kempter, *J. Chem. Phys.*, 2008, **128**, 134712.
52 R. Souda, H. Kawanowa, M. Kondo and Y. Gotoh, *J. Chem. Phys.*, 2003, **119**, 6194–6200.
53 D. Adachi, Y. Katsumoto, H. Sato and Y. Ozaki, *Appl. Spectrosc.*, 2002, **56**, 357–361.
54 S. M. Meja, J. F. Espinal and F. Mondragón, *THEOCHEM*, 2009, **901**, 186–193.
55 C. D. Keefe and Z. Istvankova, *Can. J. Chem.*, 2010, **89**, 34–46.
56 Y. Gu, T. Kar and S. Scheiner, *J. Am. Chem. Soc.*, 1999, **121**, 9411–9422.
57 P. Hobza and Z. Havlas, *Chem. Rev.*, 2000, **100**, 4253–4264.
58 U. Buck and F. Huisken, *Chem. Rev.*, 2000, **100**, 3863–3890.
59 S. K. Allison, J. P. Fox, R. Hargreaves and S. P. Bates, *Phys. Rev. B: Condens. Matter Mater. Phys.*, 2005, **71**, 024201.
60 J. A. B. da Silva, F. G. B. Moreira, V. M. L. dos Santos and R. L. Longo, *Phys. Chem. Chem. Phys.*, 2011, **13**, 6452–6461.
61 L. Dougan, S. Bates, R. Hargreaves, J. Fox, J. Crain, J. Finney, V. Reat and A. Soper, *J. Chem. Phys.*, 2004, **121**, 6456–6462.